

Extended Near-Infrared Emission from Candidate Protostars in the Taurus-Auriga Molecular Cloud

Shinae Park

Physics Department, University of California, 366 LeConte Hall, Berkeley, CA 94720-7300

and

Scott J. Kenyon

Smithsonian Astrophysical Observatory, 60 Garden Street, Cambridge, MA 02138

to appear in

The Astronomical Journal, June 2002

ABSTRACT

We describe near-IR imaging data for a sample of 23 class I sources in the Taurus-Auriga dark clouds. Combining our data with previous photometry, we detect brightness variations of ~ 0.1 – 0.5 mag in many sources. The near-IR morphologies are consistent with mm continuum measurements. Most ($\sim 60\%$) of the sample are true protostars; the rest may be objects in transition between class I and class II, T Tauri stars with edge-on disks, or heavily reddened T Tauri stars.

Subject headings: infrared: stars — stars: formation — stars: pre-main-sequence — ISM: reflection nebulae

1. INTRODUCTION

Standard models for the formation of a single, low-mass star begin with a slowly rotating cloud of gas and dust with a centrally concentrated density distribution (e.g., Larson 1969, 1972; Stahler, Shu, & Taam 1980, 1981; Shu, Adams, & Lizano 1987; Shu et al. 1993; Safier, McKee, & Stahler 1997; Ciolek & Basu 2000; Whitworth & Ward-Thompson 2001). When the inward gravitational pressure exceeds the outward thermal and magnetic pressures, the cloud collapses. Material near the axis of rotation with low specific angular momentum contracts into a central star-like core. Once the radius of the centrifugal barrier exceeds the radius of the central stellar core, material away from the rotation axis with large specific angular momentum follows a curved infall trajectory, falls onto the equatorial plane, and forms a circumstellar disk (Cassen & Moosman 1981; Terebey et al. 1984; Lin & Pringle 1990; Yorke et al. 1993; Stahler et al. 1994). As the collapse proceeds, the protostellar core becomes more massive and more luminous; the surrounding infalling

envelope becomes less massive and less opaque at optical and infrared wavelengths (Lada 1991). Eventually, a wind from the star-disk system begins to clear gas and dust away from the rotational axis, resulting in the production of collimated jets and a bipolar molecular outflow (Adams & Lin 1993; Konigl & Ruden 1993; Konigl & Pudritz 2000; Shu et al. 2000). Once the infalling envelope disperses or falls into the circumstellar disk, the central star-disk system becomes optically visible as a pre-main-sequence star. As the material in the disk accretes onto the central star, dissipates, or condenses into planets, the star moves onto the main sequence (Stahler & Walter 1993; Strom et al. 1993; Cameron 1995).

This picture of star formation generally accounts for an apparent evolutionary sequence in the observed properties of young stars in nearby molecular clouds (Lada 1984; Adams et al. 1987; Lada 1987). Lada (1991) describes three of the classes in this sequence. Class I sources have spectral energy distributions (SEDs) which are broader than a single temperature blackbody function and rise from $\sim 2 \mu\text{m}$ to $\sim 25\text{--}100 \mu\text{m}$. Class I sources are star-disk systems still surrounded by massive infalling envelopes. The envelope absorbs optical and near-infrared photons from the central protostar and re-emits this radiation at far-IR and mm wavelengths where the envelope is optically thin. Class II sources also have broad SEDs, but the SED falls from $\sim 2 \mu\text{m}$ to $\sim 25\text{--}100 \mu\text{m}$. These sources contain a pre-main-sequence star surrounded by a circumstellar disk, which absorbs and reradiates emission from the central star. Class III sources have roughly blackbody SEDs that peak at $\sim 1 \mu\text{m}$; radiation from a surrounding disk or envelope contributes negligible emission at $10\text{--}100 \mu\text{m}$ (Lada 1991). André et al. (1993) added the class 0 sources to this sequence to include very young objects at the beginning of the accretion process. These objects have narrow SEDs which peak at $\sim 100\text{--}300 \mu\text{m}$ (e.g., Motte & André 2001, and references therein). In the current picture, the central star of a class 0 source has accumulated $\lesssim 50\%$ of its final mass; in class I sources, the central star has $\gtrsim 50\%$ of its final mass.

The Taurus-Auriga cloud is one of the best sites for testing models of isolated, low mass star formation (see Kenyon & Hartmann 1995, and references therein). This collection of filamentary clouds contains good samples of class I, II, and III pre-main sequence stars, a class 0 source, and several examples of interesting transition objects. The clouds are close enough ($d = 140$ pc; Kenyon, Dobrzycka, & Hartmann 1994a) to allow high signal-to-noise observations at all wavelengths with moderate to high spectral and spatial resolution. Although the clouds are poor examples of clustered star formation, pre-main sequence stars in Taurus-Auriga provide interesting constraints on the formation of small close groups of pre-main sequence stars (Gómez et al. 1993; Armitage & Clarke 1997; Vanhala & Cameron 1998; Scalo & Chappell 1999).

Here, we consider a comparison between the millimeter (mm) and near-infrared (near-IR) properties of class I sources in Taurus-Auriga. Motte & André (2001) demonstrate that moderate spatial resolution mm continuum observations divide these objects into unresolved, point-like sources with negligible infalling envelopes, extended sources with significant infalling envelopes, and several transition objects with modest infalling envelopes. In this division, the unresolved Taurus-Auriga sources might be edge-on disks similar to those discovered in HH30 IRS and HK

Tau (Burrows et al. 1996; Stapelfeldt et al. 1998). Because the derived lifetimes in each evolutionary phase depend on the relative numbers of objects in each phase (e.g. Kenyon et al. 1990; Hogerheijde 2001), the mm continuum data also provide better limits on the class I lifetime in Taurus-Auriga. Our goal is to test whether near-IR images yield a similar division of sources into extended and point-like objects. This study extends previous imaging surveys, where near-IR imaging data constrains radiative transfer models for the class I sample (Kenyon et al. 1993b; Whitney et al. 1997).

We describe the observations in §2, comment on source variability in §3, and consider the image morphology in §4. The paper concludes with a brief summary.

2. OBSERVATIONS

We acquired JHK images of candidate protostars in Taurus-Auriga with Stelircam at the Fred L. Whipple Observatory 1.2-m telescope on 5–12 October 1998 and 18–20 November 1999. Stelircam is a dual-beam IR imager equipped with two 256×256 InSb SBRC arrays. The field-of-view for these images is $\sim 300'' \times 300''$. We took nine 6×10 sec exposures of each field at HK and later at JK and offset the telescope by $45''$ – $60''$ after each integration. Poor weather prevented a complete set of J band observations in photometric conditions; the 1998 HK observations were photometric. We repeated observations of some targets to improve the signal-to-noise of faint nebulosity.

We produce calibrated object frames in each filter using standard techniques in the Interactive Data Language (IDL)¹. After correcting each image for non-linearity, we construct a nightly flat-field for each filter from the median of dark-subtracted image frames. The sky frames for each object image are a median-filtered set of flattened frames scaled to have the same background as the object image. We offset and coadd the nine frames in each filter to make a final deep field image which reveals fainter extended emission without saturating bright stars.

Table 1 lists HK photometry for each source. We use the NOAO IRAF² routine PHOT to extract magnitudes in three apertures. We analyze the nine HK frames of each source – instead of the coadded frames – to obtain error estimates for the photometry directly from the data. Once we remove bad pixels, the typical standard deviation of nine measurements for one source is ± 0.01 – 0.02 mag at K and ± 0.02 – 0.03 mag at H. Our nightly photometric calibration is based on 15–25 observations of Elias et al. (1982) standard stars. The uncertainty in the calibration is ± 0.03 mag in each filter on each night. This uncertainty is comparable to the range in the zero-points and airmass corrections for the HK filters on each observing run. Adding the calibration error in quadrature with the standard deviations of the source data yields a typical photometric error of

¹IDL is distributed by Research Systems, Inc. of Boulder, Colorado.

²IRAF is distributed by the National Optical Astronomy Observatory, which is operated by the Association of Universities for Research in Astronomy, Inc. under contract to the National Science Foundation.

less than 0.05 mag in each filter.

To measure morphological information from the individual and coadded frames, we use Sextractor (Bertin & Arnouts 1996). Sextractor is a modern software package which automatically detects, measures, and classifies sources from digital images. For each image, we set up the package to measure the FWHM f , elongation e , central surface brightness μ , and the magnitude in $7''$ and $14''$ apertures for each candidate protostar. Table 2 lists the results. The FWHM is the full width at half maximum of the best-fitting one dimensional gaussian to the intensity profile of the source; the elongation is the ratio of the major axis to the minor axis of the best-fitting two dimensional gaussian to the intensity profile. The fits for both parameters use intensity levels 3σ or more above the local noise background. We use the central surface brightness and aperture magnitudes to verify that fits for each source reach the same limiting surface brightness and to check the PHOT photometry. The Sextractor photometry agrees with PHOT to ± 0.02 mag or better. The limiting surface brightness in the coadded frames is ~ 19.5 mag arcsec $^{-2}$.

Figure 1 gives examples of contour maps derived from coadded K band images for Taurus-Auriga protostars (see also Tamura et al. 1991; Kenyon et al. 1993b; Whitney et al. 1997; Lucas & Roche 1997). The images have a variety of morphologies, ranging from apparent point sources (04108+2803 and 04295+2251) to monopolar (04287+1801 and 04288+1802) and bipolar (04325+2402 and 04361+2547) nebulae with central point sources. Two objects are faint patches with no obvious point source (04166+2706 and 04368+2557). Whitney et al. (1997) measure large near-IR polarizations for sources with extended nebulae, confirming models where dust grains within the nebulosity scatter radiation from the central star into our line-of-sight (see also Lucas & Roche 1998a). Gómez et al. (1997) identify optical and near-IR jets on [S II] and H $_2$ images of many Taurus-Auriga protostars (see also Lucas & Roche 1998b); Kenyon et al. (1998) note [S II] emission on optical spectra of several other sources. Jet emission and bipolar outflows are characteristic of embedded protostars (e.g., Reipurth 1991; Moriarty-Schieven et al. 1992; Bontemps et al. 1996; Tamura et al. 1996; Reipurth & Bally 2001).

The IRAS source 04166+2706 deserves special mention. Kenyon et al. (1990) discovered a near-IR counterpart with raster scans on the single channel MMT photometer. From near-IR imaging data, Kenyon et al. (1993b) identified a point source with very red colors near the IRAS position. This object is ~ 2 mag brighter than the Kenyon et al. (1990) source and lies near the reddening band in the J–K,H–K color-color diagram. Our images recover the Kenyon et al. (1990) source as a patch of low surface brightness nebulosity similar to the nebula of 04368+2557 (see Whitney et al. 1997). This object is $52''$ N and $44''$ W of the Kenyon et al. (1993b) point source, with J2000 coordinates of RA = $04^{\text{h}}19^{\text{m}}43.2^{\text{s}}$ and Dec = $+27^{\circ}13'39''$. The error in these coordinates is roughly $\pm 2''$. We suggest that this object is the IRAS counterpart.

The triplet of embedded sources associated with IRAS sources 04181+2654 and 04181+2655 also merit a short comment. Kenyon et al. (1993a, 1993b) associate the northern component with IRAS 04181+2655 and the southern pair with IRAS 04181+2654. In this convention, the southern

embedded source is 04181+2654A; the middle component of the three is 04181+2654B. Figure 1 labels these three sources. For completeness, the J2000 coordinates are RA = $04^{\text{h}}21^{\text{m}}11.6^{\text{s}}$ and Dec = $+27^{\circ}01'10''$ for 04181+2654A, RA = $04^{\text{h}}21^{\text{m}}10.5^{\text{s}}$ and Dec = $+27^{\circ}01'38''$ for 04181+2654B, and RA = $04^{\text{h}}21^{\text{m}}08.1^{\text{s}}$ and Dec = $+27^{\circ}02'22''$ for 04181+2655.

3. Variability

Most pre-main sequence stars vary at optical and infrared wavelengths (e.g., Joy 1945; Bouvier et al. 1993; Choi & Herbst 1996; Stassun et al. 1999). Many systems have regular variations with amplitudes of 0.1–1.0 mag and periods of 2–10 days (Eaton, Herbst, & Hillenbrand 1995; Herbst et al. 1994, 2000). Other objects vary irregularly with similar amplitudes on similar or longer timescales. The periodic variations yield information on stellar rotational periods and the sizes, temperatures, and lifetimes of dark and bright spots on the stellar photosphere (Bouvier et al. 1993; Stassun et al. 1999). These data also provide tests of models for the inner disks and magnetospheres of low mass pre-main sequence stars (e.g., Mahdavi & Kenyon 1998; Wood & Whitney 1998; Wood et al. 2000).

To test whether any of the candidate protostars are variable, we compare with previous measurements obtained with single channel photometers (Kenyon et al. 1990) and near-IR imagers (Kenyon et al. 1993b, 1994b; Whitney et al. 1997). For sources where we have only one or two of our own measurements, we supplement the photometry with data from the compilation of Kenyon & Hartmann (1995). We derive the average brightness and the standard deviation for the candidate protostar and for another stellar source in the same field using $8''$ and $13''$ – $14''$ apertures. Although there are too few measurements for each source to construct a robust average, the standard deviation provides a reasonable first estimate of source variability.

The observations in this study use different instruments; we use the comparison stars to verify that the photometry from each instrument is on the same magnitude scale. We could not perform this test with single channel photometry; previous comparisons show that the differences between photometric systems are small compared to the source variations in our sample (Kenyon & Hartmann 1995). As a final test, we check whether the mean variation of a protostar from one observing run to the next is zero. Using data from Kenyon et al. (1993b), Whitney et al. (1997), and this paper, the average change in brightness of the complete sample is 0.11 ± 0.37 from 1991 to 1993–94 and 0.05 ± 0.31 from 1993–94 to 1998–99.

Our analysis indicates that candidate protostars in Taurus-Auriga are variable. Histograms of standard deviations σ in K and in H–K (Figure 2) demonstrate that candidate protostars have larger variations than comparison stars in the same field. The variation of a typical source has an amplitude of 0.2–0.3 mag at K. These fluctuations are similar to variations observed in optically visible T Tauri stars (e.g., Kenyon & Hartmann 1995; Choi & Herbst 1996; Stassun et al. 1999).

Many sources have variable colors. Roughly half of the sample varied by 0.1–0.3 mag in H–K. Although large color variations are observed in some T Tauri stars, the variations are less than 0.1–0.2 mag in more than 70% of pre-main sequence stars in Taurus-Auriga (Kenyon & Hartmann 1995, see also Carpenter, Hillenbrand, & Skrutskie 2001).

Without repeat observations on short timescales, we are unable to analyze the variability of Taurus-Auriga protostars in detail. The large brightness and color changes are consistent with the behavior expected from bright spots, dark spots, and obscuration models (see also Carpenter et al. 2001, and references therein). There is no correlation between brightness and color changes; some sources become bluer as they brighten while others become redder. Most models predict strong correlations between color and brightness evolution, but our observations are too few in number to discriminate between possible models.

The variations of several objects deserve special mention.

04018+2803B – This source is the more embedded of a pair of *IRAS* sources separated by $17''5$ on the sky. The large variation is based on a single observation in October 1998.

04181+2655 – The brightest of a triplet of *IRAS* sources, this object has varied consistently from one observing run to the next. The color variation of this source is among the largest in our sample.

04239+2436 – This source has a large nebulosity at J which is nearly invisible at K. It has one of the largest amplitudes in our sample, with a variation of more than 0.7 mag at K during the past decade.

Six other sources – 04016+2610, 04181+2654A, 04287+1801 (L1551 IRS5), 04361+2547, 04365+2535, and 04381+2540 – vary by 20% or more in brightness and in color. All other sources change by less than 0.1–0.2 mag (Table 1; columns 10–11). The historical variation of L1551 IRS5 is difficult to quantify due to large differences in observing techniques, but published data are consistent with the variation in our data.

4. Morphology

Image morphology provides a good constraint on models for embedded protostars. Whitney et al. (1997) demonstrate that the size of synthetic near-IR images correlates with the centrifugal radius R_c and the infall rate \dot{M} in the Terebey et al. (1984) infalling envelope model. The elongation correlates with the inclination of the source and the size of the outflow cavity (see also Whitney & Hartmann 1993). Both parameters vary with the grain albedo. Grains with large albedo produce larger and more elongated near-IR images of protostars. Whitney et al. (1997) emphasize that the size and elongation provide better constraints on models when combined with polarization measurements.

The image morphology also provides a good comparison with mm continuum observations.

Motte & André (2001) describe moderate spatial resolution mm-wave observations of the Taurus-Auriga sample. They divide the sources into two groups based on the ratio of the flux F in $11''$ and $60''$ beams. Extended sources have $F_{11}/F_{60} \lesssim 0.5\text{--}0.7$; point sources have $F_{11}/F_{60} \approx 1$. Roughly half of the Taurus-Auriga sample is extended by this criterion.

To compare the near-IR morphology with mm continuum morphology, we use two measures to divide objects into extended sources and point-like sources. We follow Motte & André (2001) and define extended sources as objects where the flux in a $26''$ aperture exceeds the fluxes in $13''$ and $8''$ apertures (Table 1). Larger apertures yield poor quality photometry on our images. In a sample of ~ 2000 field stars with moderate signal-to-noise photometry, the mean aperture corrections for our data are $m_8\text{--}m_{13} = 0.09\pm 0.02$ and $m_{13}\text{--}m_{26} = 0.11\pm 0.02$. The aperture corrections are independent of the filter. With this result, extended sources have $m_8\text{--}m_{13} > 0.15$ and $m_{13}\text{--}m_{26} > 0.17$. The size (FWHM) f and elongation e also provide good measures of source extension. In a sample of ~ 3000 moderate signal-to-noise detections from our K-band images, the median size is $f_{med} = 1''.75\pm 0''.30$ where the error bar refers to the inter-quartile range (Figure 3). The median elongation in the K-band images is $e_{med} = 1.10\pm 0.04$. Point sources are well-defined in our images. We thus define extended sources to have $f_K > 2''.5$ and $e_K > 1.2$.

Our analysis indicates a good correlation between various measures for extended emission in the Taurus-Auriga class I sample (Figure 4). For sources with $f_K \leq 5''$, there is a one-to-one relation between f_K and $K_8\text{--}K_{13}$ (Figure 4; lower left panel). Although this relation is weaker at larger sizes, the Spearman rank order test (Press et al. 1988) still indicates a significant correlation with a probability, $p_s \approx 3 \times 10^{-4}$, of being drawn from a random sample. The elongation and size derived from SExtractor show a stronger correlation (Figure 4, lower right panel), with $p_s \approx 5 \times 10^{-5}$.

The good correlation between size and elongation confirms predictions of radiative transfer models for protostars with infalling envelopes. In the Terebey et al. (1984) infall models with a bipolar outflow cavity, the size and the elongation of near-IR images are related to infall rate and the geometry of the outflow cavity. Protostars with denser envelopes, larger infall rates, and curved or dust-filled outflow cavities are larger and more elongated than protostars with less dense envelopes, smaller infall rates, or streamline cavities (Kenyon et al. 1993b; Whitney et al. 1997). Our data confirm the general correlation predicted by the models. Further comparisons between the data and the models will yield better tests of the models.

The K-band size and elongation are well-correlated with the mm continuum measurements. Motte & André (2001) define the concentration c as the ratio of the fluxes in $11''$ and $60''$ apertures expressed as a percentage. Highly concentrated sources have $c = 100$; very extended sources have $c < 30$. Our near-IR measures f_K and e_K are inversely correlated with c (Figure 4, middle panels). The relation between c and e_K is significant at the 3σ level, with $p_s \approx 4 \times 10^{-3}$; the size is more weakly correlated with c ($p_s \approx 10^{-2}$). Motte & André (2001) use the concentration and the absolute fluxes to measure the envelope mass, M_{env} . Our K-band measures are more strongly correlated

with M_{env} than with c (Figure 4, upper panels); $p_s \approx 2 \times 10^{-3}$ is the Spearman rank probability for the correlation between f_K and M_{env} and $p_s \approx 10^{-3}$ is the probability for the correlation between e_K and M_{env} .

The near-IR measurements at J and H also correlate with the mm continuum data. Because the short wavelength images have lower signal-to-noise, the correlations at J and H are 10% to 20% weaker than at K. These results exclude the deeply embedded source 04368+2557 (L1527 IRS) from the analysis. Including this source with a nominal size of $f_K \approx 25''$ and an elongation of $e_K \approx 2$ yields smaller Spearman rank probabilities by a factor of 2–3.

These correlations provide additional confirmation of infall models for protostars. In the standard infall picture (Terebey et al. 1984; Adams et al. 1987), an optically thick envelope absorbs radiation from the central object and re-radiates this energy at mm wavelengths. Protostars with massive infalling envelopes are therefore more extended at mm continuum wavelengths than class II or class III sources with little or no infalling envelope. Once the central object generates a bipolar outflow, optical and near-IR radiation from the central object can escape through the optically thin cavity (e.g. Whitney & Hartmann 1993; Kenyon et al. 1993b; Whitney et al. 1997). Some of this radiation scatters off material in the cavity and in the outer envelope, producing an extended, elongated, and highly polarized optical or near-IR image (Whitney et al. 1997). As material from the envelope continues to fall onto the disk, the envelope opacity declines and more optical and IR radiation from the central star can reach the observer directly. This process reduces the amount of mm continuum emission and scattered optical and near-IR emission. These objects thus appear more concentrated and more symmetrical at all wavelengths than more highly embedded objects. Our data confirm this general trend: class I sources that are extended at mm continuum wavelengths are extended and more elongated on near-IR images than their point-like counterparts.

These correlations may also offer a test of infalling envelope models. To the best of our knowledge, there are few quantitative predictions of the relationship between the optical or near-IR properties and the mm continuum properties of protostars. Published radiative transfer models have successfully modeled independently the spectral energy distributions, density distributions, and near-IR images of individual protostars. However, we are not aware of models that predict the observed correlations between the concentration or envelope mass derived from mm data and the size or elongation derived from optical or near-IR data. Our results suggest that observations can now test these predictions.

The near-IR data divide Taurus-Auriga class I sources into nearly the same two groups as the mm continuum data. We base this conclusion on Table 3, which compares our results with those of Motte & André (2001). Nine sources are extended at mm and near-IR wavelengths; eight sources are not extended at these wavelengths. Two sources – 04016+2610 and 04302+2247 – have large near-IR nebulae with little evidence for extended millimeter continuum emission from

a massive envelope³ (Hogerheijde 2001; Motte & André 2001). Three sources – 04181+2654A, 04181+2654B, 04365+2535, and 04381+2540 – are extended at mm continuum wavelengths but are not extended at near-IR wavelengths based on our measurements of size and elongation. Three of these – 04181+2654A, 04365+2535, and 04381+2540 – show some evidence for an extended nebula at K from K_8 – K_{13} and a visual inspection of the coadded images (see Figure 1). Higher signal-to-noise K-band images would provide definitive tests for extended emission in these sources.

Our data confirm the Motte & André (2001) conclusion that most ($\sim 60\%$) of the Taurus-Auriga class I sources are embedded protostars with massive infalling envelopes (see also Hogerheijde et al. 1998; Hogerheijde & Sandell 2000; Chandler & Richer 2000, and references therein). Because these objects are definitely extended in the mm continuum and probably extended at K, we include 04181+2654A, 04181+2654B, and 04381+2540 in this group (see Table 2). The envelope masses inferred from the millimeter data range from $\sim 0.09 M_\odot$ for 04239+2436 to $\sim 0.9 M_\odot$ for L1551 IRS5. The density distributions for these sources, $\rho(r) \propto r^{-n}$ with $n = 1.5$ – 2 , agree with the predictions of infall models on scales of $\sim 10,000$ AU (Terebey et al. 1984; Chandler, Barsony, & Moore 1998; Hogerheijde et al. 1998; Hogerheijde & Sandell 2000; Motte & André 2001). The SEDs and the near-IR morphologies and polarizations of these sources also agree with model predictions (Kenyon et al. 1993a,b; Whitney et al. 1997; Motte & André 2001). All of these sources have molecular outflows (e.g., Bontemps et al. 1996) and 66% have emission from optical or near-IR jets (e.g., Gómez et al. 1997).

At least two Taurus-Auriga class I sources without extended mm emission might be transition objects between class I protostars and class II T Tauri stars. In addition to their large near-IR nebulae, 04016+2610 and 04302+2247 have molecular outflows, optical or near-IR emission from a jet, and large near-IR polarization as in true protostars (see also Heyer et al. 1990; Tamura et al. 1991; Kenyon et al. 1993b; Gómez et al. 1997; Whitney et al. 1997). However, both sources fail to meet the “true protostar” criterion of Motte & André (2001), $M_{env}/M_\star \gtrsim 0.1$. To estimate these ratios in 04016+2610 and 04302+2247, we assume the central star in each source lies on the birthline of Palla & Stahler (1999). The observed bolometric luminosities then yield approximate stellar masses of $M_\star \sim 0.6 M_\odot$ for 04016+2610 and $M_\star \lesssim 0.1 M_\odot$ for 04302+2247. Motte & André (2001) estimate envelope masses $M_{env} \lesssim 0.04 M_\odot$ for 04016+2610 and $M_{env} \lesssim 0.01 M_\odot$ for 04302+2247. Thus, both sources have $M_{env}/M_\star \lesssim 0.1$ and are not true protostars.

Based on mm aperture synthesis observations, Hogerheijde (2001) previously proposed that 04016+2610 is a transition object between true protostars and class II sources. The mm data are consistent with a Keplerian disk with a radius of ~ 2000 AU surrounding a $0.65 M_\odot$ central star (see also Saito et al. 2001). Our mass estimate favors this interpretation over the proposal of sub-Keplerian motion around a more massive star. If 04016+2610 is a transition object, several

³04016+2610 is resolved at 2 cm and 3.5 cm (Lucas, Blundell, & Roche 2000); this emission probably traces radiation from an ionized jet or inner disk as in L1551 IRS5 (Rodríguez et al. 1986).

common near-IR properties suggest that 04302+2247 might also be a transition object⁴. Aperture synthesis observations at mm wavelengths would test this proposal.

Other Taurus-Auriga class I sources are peculiar in having class I SEDs but little or no extended near-IR or mm continuum emission. The properties of this group differ significantly from the true protostars. Most do not have molecular outflows, optical/near-IR jet emission, or large near-IR polarization. As a group, these objects thus appear older, with smaller extended envelopes and less accretion activity than the protostars (see also Reipurth & Bally 2001). There are several exceptions to this statement. Four sources – 04158+2805, 04260+2642, 04264+2433, and 04489+3042 – have [S II] emission; 04264+2433 has large near-IR polarization; near-IR spectra of 04295+2251 and 04489+3042 more closely resemble spectra of class I sources than T Tauri stars Greene & Lada (1996). This diversity of properties suggests that the peculiar class I sources do not belong to a single class of objects.

Table 2 lists our best estimates for the nature of these peculiar class I sources. We consider 04016+2610, 04260+2612, 04264+2433, 04302+2247 as transition objects between class I and class II. Extended, highly polarized near-IR nebulae demonstrate that 04016+2610 and 04302+2247 are not class II sources; 04181+2655, 04260+2612 and 04264+2433 have similar spectral energy distributions but no obvious near-IR nebulosity. The class I sources 04108+2803B, 04295+2251, and 04489+3042 have larger optical to far-IR flux ratios than 04016+2610 and other ‘transition candidates.’ These sources could be transition objects viewed along the rotational axis of the disk. The strong [S II] emission in 04295+2251 recalls similar emission in the edge-on disk systems HK Tau and HH30 IRS. Finally, 04108+2803A and 04158+2805 are more similar to class II sources and are probably heavily reddened T Tauri stars.

5. SUMMARY

Our near-IR observations provide a first detection of near-IR variability in a sample of class I protostars. The variations are similar in amplitude to those observed in T Tauri stars (Kenyon & Hartmann 1995; Carpenter et al. 2001). The poor time coverage of the imaging data for this sample does not provide a useful measure of the timescale for these variations. If the variations are similar to those in T Tauri stars, observations on successive nights over weeks or months can measure the timescales. As an example, Hillenbrand et al. (2001) derive an 8 day period for the variation in the Becklin-Neugebauer object, an embedded protostar in Orion (see also Wood et al. 2000).

The near-IR morphologies of Taurus-Auriga class I sources are consistent with the mm contin-

⁴Padgett et al. (1999) detect an edge-on disk on HST near-IR images of 04302+2247, but our ground-based near-IR images of 04302+2247 show more near-IR nebulosity than class II sources with edge-on disks such as HH30 IRS and HK Tau.

uum measurements of Motte & André (2001). Most ($\sim 60\%$) of these objects are true protostars, with massive envelopes surrounding a young star with $\sim 50\%$ of its final mass. Some ($\sim 25\%$) of the class I sources are probably transition objects between true protostars and optically visible T Tauri stars; one or two of these might have edge-on disks similar to those observed in HH30 IRS and HK Tau. Two other class I sources are probably heavily reddened T Tauri stars;

Making accurate classifications for the “peculiar” class I sources requires additional data. Radio observations of some class I sources using higher spatial resolution might reveal compact nebulae or large disks as in 04016+2610 (Hogerheijde 2001). Deeper near-IR images may also reveal extended nebulosity. We have marginal detections of faint nebulosity on coadded near-IR images of 04181+2655 and 04264+2433; higher signal-to-noise observations might provide a better indication of the extended nature of these and other point-like class I sources. Because molecular outflows and optical/near-IR jets are more common among class I sources and transition objects than among T Tauri stars with class II SEDs (Gómez et al. 1997; Kenyon et al. 1998; Reipurth & Bally 2001), deeper optical and near-IR surveys for jet emission and more extensive outflow surveys can also help to classify these objects. These new data would provide a better understanding of the evolution from class I to class II among low mass protostars.

Finally, our results offer a new test of infall models for class I protostars. In the standard picture, a massive envelope produces mm and far-IR continuum emission; near-IR and optical radiation from the central object escape through the optically thin outflow cavity. As the infalling envelope becomes less massive and less opaque, the angular size of the outflow cavity should shrink. Because optical and near-IR radiation can escape the envelope more easily, protostars should become less elongated as the optical depth through the envelope decreases. Our near-IR morphological data confirm this expectation: f_K and e_K of class I sources correlate with M_{env} . The standard model also predicts a general anti-correlation between the near-IR measurements f_K and e_K and the mm measurement c of Motte & André (2001). As the envelope mass declines, the unresolved central star and the disk produce more of the mm continuum flux; sources thus become more concentrated at mm wavelengths as they become less elongated and less extended at optical and near-IR wavelengths. To the best of our knowledge, however, theoretical radiative transfer models of protostars do not make specific predictions for the variation of f_K or e_K as a function of c or M_{env} . Our results demonstrate that near-IR and mm continuum data can test these predictions.

We thank C. Lada for advice and comments on this project. M. Geller and an anonymous referee made many useful comments on the manuscript. W. Wyatt and J. Grimes provided technical assistance. S. P. thanks the National Science Foundation for their support of the REU program at the Smithsonian Astrophysical Observatory where most of this work was carried out. S. K. thanks Dr. S. Starrfield and Arizona State University for their hospitality during the completion of this project.

REFERENCES

- Adams, F. C., Lada, C. J., & Shu, F. H. 1987, *ApJ*, 321, 788
- Adams, F. C., & Lin, D. N. C. 1993, in *Protostars and Planets III*, ed. E.H. Levy & J.I. Lunine (Tucson: Univ. Arizona), p. 721
- André, P., Ward-Thompson, D., & Barsony, M. 1993, *ApJ*, 406, 122
- Armitage, P. J., & Clarke, C. J. 1997, *MNRAS*, 285, 540
- Bertin, E. & Arnouts, S. 1996, *A&AS*, 117, 393
- Bontemps, S., André, P., Terebey, S., & Cabrit, S. 1996, *A&A*, 311, 858
- Bouvier, J., Cabrit, S., Fernandez, M., Martin, E. L., & Matthews, J. M. 1993, *A&A*, 272, 176
- Burrows, C. J., et al. 1996, *ApJ*, 473, 437
- Cameron, A. G. W. 1995, *Meteoritics*, 30, 133
- Carpenter, J. M., Hillenbrand, L. A., & Skrutskie, M. F. 2001, *AJ*, 121, 3160
- Cassen, P., & Moosman, A. 1981, *Icarus*, 48, 353
- Chandler, C. J., Barsony, M. & Moore, T. J. T. 1998, *MNRAS*, 299, 789
- Chandler, C. J., & Richer, J. S. 2000, *ApJ*, 530, 851
- Choi, P. L., & Herbst, W. 1996, *AJ*, 111, 283
- Ciolek, G. E., & Basu, S. 2000, *ApJ*, 529, 925
- Eaton, N. L., Herbst, W. & Hillenbrand, L. A. 1995, *AJ*, 110, 2369
- Elias, J. H., Frogel, J. A., Matthews, K., & Neugebauer, G. 1982, *AJ*, 87, 1029
- Gómez, M., Hartmann, L., Kenyon, S. J., & Hewett, R. 1993, *AJ*, 105, 1927
- Gómez, M., Kenyon, S. J., & Whitney, B. A. 1997, *AJ*, 114, 1138
- Greene, T. P., & Lada, C. J. 1996, *AJ*, 112, 2184
- Gullbring, E., Calvet, N., Muzerolle, J., & Hartmann, L. 2000, *ApJ*, 544, 927
- Herbst, W., Herbst, D. K., Grossman, E. J., & Weinstein, D. 1994, *AJ*, 108, 1906
- Herbst, W., Rhode, K. L., Hillenbrand, L. A., & Curran, G. 2000, *AJ*, 119, 261
- Heyer, M.H., Ladd, E.F., Myers, P.C., & Campbell, B. 1990, *AJ*, 99, 1585

- Hillenbrand, L. A., Carpenter, J. M., & Skrutskie, M. F. 2001, *ApJ*, 547, L53
- Hogerheijde, M. R. 2001, *ApJ*, 553, 618
- Hogerheijde, M. R. & Sandell, G. 2000, *ApJ*, 534, 880
- Hogerheijde, M. R., van Dishoeck, E. F., Blake, G. A., & van Langevelde, H. J. 1998, *ApJ*, 502, 315
- Joy, A. H. 1945, *ApJ*, 102, 168
- Kenyon, S. J., Brown, D. I., Tout, C. A., & Berlind, P. 1998, *AJ*, 115, 2491
- Kenyon, S. J., Calvet, N., & Hartmann, L. 1993a, *ApJ*, 414, 676
- Kenyon, S. J., Dobrzycka, M., & Hartmann, L. 1994a, *AJ*, 108, 1872
- Kenyon, S. J., Gomez, M., Marzke, R. O., & Hartmann, L. 1994b, *AJ*, 108, 251
- Kenyon, S. J., & Hartmann, L. 1995, *ApJS*, 101, 117
- Kenyon, S. J., Hartmann, L.W., Strom, K.M., & Strom, S.E. 1990, *AJ*, 99, 869
- Kenyon, S. J., Whitney, B.A., Gómez, M., & Hartmann, L. 1993b, *ApJ*, 414, 773
- Königl, A., & Ruden, S. P. 1993, in *Protostars and Planets III*, ed. E. H. Levy & J. I. Lunine (Tucson: Univ. Arizona), p. 641
- Königl, A., & Pudritz, R. E. 2000, in *Protostars and Planets IV*, ed. V. Mannings, A. Boss, & S. Russell (Tucson: Univ. Arizona), p. 759
- Lada, C. J., & Wilking, B. A. 1984, *ApJ*, 287, 610
- Lada, C. J. 1987, in *Star Forming Regions*, ed. M. Peimbert & J. Jugaku (Dordrecht: Reidel), p. 1
- Lada, C. J. 1991, in *The Physics of Star Formation and Early Stellar Evolution*, ed. C. J. Lada & N. D. Kylafis (Dordrecht: Kluwer), p. 329
- Larson, R. B. 1969, *MNRAS*, 145, 271
- Larson, R. B. 1972, *MNRAS*, 157, 121
- Lin, D. N. C., & Pringle, J. E. 1990, *ApJ*, 357, 113
- Lucas, P. W., Blundell, K. M., & Roche, P. F. 2000, *MNRAS*, 318, 526
- Lucas, P. W., & Roche, P. F. 1997, *MNRAS*, 286, 895
- Lucas, P. W., & Roche, P. F. 1998, *MNRAS*, 299, 699

- Lucas, P. W., & Roche, P. F. 1998, MNRAS, 299, 723
- Mahdavi, A., & Kenyon, S. J. 1998, ApJ, 497, 342
- Moriarty-Schieven, G. H., Wannier, P. G., Tamura, M., & Keene, J. 1992, ApJ, 400, 260
- Motte, F., & André, P. 2001, A&A, 365, 440
- Padgett, D. L., et al. 1999, AJ, 117, 1490
- Palla, F., & Stahler, S. W. 1999, ApJ, 525, 772
- Press, W. H., Flannery, B. P., Teukolsky, S. A., & Vetterling, W. T. 1988, *Numerical Recipes, The Art of Scientific Computing*, Cambridge, Cambridge
- Reipurth, B. 1991, in *Physics of Star Formation and Early Stellar Evolution*, ed. C. J. Lada & N. D. Kylafis, Dordrecht, Kluwer, p. 497
- Reipurth, B., & Bally, J. 2001, ARA&A, 39, 403
- Rodriguez, L. F., Canto, J., Torrelles, J. M., & Ho, P. T. P. 1986, ApJ, 301, L25
- Safier, P. N., McKee, C. F. & Stahler, S. W. 1997, ApJ, 485, 660
- Saito, M., Kawabe, R., Kitamura, Y., & Sunada, K. 2001, ApJ, 547, 840
- Scalo, J., & Chappell, D. 1999, ApJ, 510, 258
- Shu, F. H., Adams, F. C., & Lizano, S. 1987, ARA&A, 25, 23
- Shu, F., Najita, J., Galli, D., Ostriker, E., & Lizano, S. 1993, in *Protostars and Planets III*, ed. E.H. Levy & J.I. Lunine (Tucson: Univ. Arizona), p. 3
- Shu, F., Najita, J. R., Shang, H., & Li, Z.-Y. 2000, in *Protostars and Planets IV*, ed. V. Mannings, A. Boss, & S. Russell (Tucson: Univ. Arizona), p. 789
- Stahler, S. W., Shu, F. H., & Taam, R. E. 1980, ApJ, 241, 637
- Stahler, S. W., Shu, F. H., & Taam, R. E. 1981, ApJ, 248, 797
- Stahler, S. W., Korycansky, D. G., Brothers, M. J., & Toulma, J. 1994, ApJ, 431, 341
- Stahler, S. W., & Walter, F. M. 1993, in *Protostars and Planets III*, ed. E. H. Levy & J. I. Lunine (Tucson: Univ. Arizona), 405
- Stapelfeldt, K., Krist, J. E., Ménard, F., Bouvier, J., Padgett, D. L., & Burrows, C. J. 1998, ApJ, 502, L65
- Stassun, K., Mathieu, R. D., Mazeh, T., & Vrba, F. J. 1999, AJ, 117, 2941

- Strom, S. E., Edwards, S., & Skrutskie, M. F. 1993, in *Protostars and Planets III*, ed. E. H. Levy & J. I. Lunine (Tucson: Univ. Arizona), p. 837
- Tamura, M., Gatley, I., Waller, W., & Werner, M.W. 1991, *ApJL*, 374, L25
- Tamura, M., Ohashi, N., Hirano, N., Itoh, Y., & Moriarty-Schieven, G. H. 1996, *AJ*, 112, 2076
- Terebey, S., Shu, F. H., & Cassen, P. 1984, *ApJ*, 286, 529
- Vanhala, H., & Cameron, A. G. W. 1998, *ApJ*, 508, 291
- Whitney, B. A., & Hartmann, L. 1993, *ApJ*, 402, 605
- Whitney, B. A., Kenyon, S. J., & Gómez, M. 1997, *ApJ*, 485, 703
- Whitworth, A. P., & Ward-Thompson, D. 2001, *ApJ*, 547, 317
- Wood, K., Stanek, K. Z., Wolk, S., Whitney, B., & Stassun, K. 2000, *ApJ*, 542, L21
- Wood, K., & Whitney, B. 1998, *ApJ*, 506, L43
- Yorke, H. W., Bodenheimer, P., & Laughlin, G. 1993, *ApJ*, 411, 274

Table 1. Photometry of Taurus-Auriga candidate protostars

IRAS Name	Other ID	JD	8'' aperture		13'' aperture		26'' aperture		σ_K	σ_{H-K}
			K	H-K	K	H-K	K	H-K		
04016+2610	L1489 IRS	51093.9	9.45	2.14	9.20	1.92	9.10	1.89	0.21	0.21
04108+2803A	L1495 IRS	51092.9	10.44	1.11	10.32	1.14	10.33	1.14	0.04	0.07
04108+2803B	L1495 IRS	51092.9	10.70	2.19	10.55	2.25	10.52	2.31	0.52	0.18
04158+2805	...	51092.9	11.03	1.04	10.90	1.02	10.86	1.02	0.16	0.06
04166+2706	...	51093.9	15.05	...	14.27	...	13.65
04169+2702	...	51093.9	11.40	2.45	11.17	2.24	11.01	1.95	0.11	0.13
04181+2655	...	51092.9	9.89	1.54	9.76	1.50	9.72	1.49	0.45	0.31
04181+2654B	...	51092.9	11.24	2.71	11.06	2.76	10.98	2.70	0.19	0.09
04181+2654A	...	51092.9	10.52	2.23	10.31	2.25	10.24	2.20	0.24	0.09
04239+2436	...	51093.9	10.33	2.47	10.17	2.35	10.12	2.20	0.31	0.06
04248+2612	HH31 IRS2	51093.9	10.60	0.70	10.17	0.65	9.91	0.69	0.13	0.05
04260+2642	...	51093.9	11.53	1.14	11.45	1.15	11.42	1.17	0.27	0.13
04264+2433	Elias 6	51092.9	11.23	0.82	11.07	0.76	10.98	0.79	0.18	0.12
04287+1801	L1551 IRS5	51092.9	9.52	1.47	9.33	1.39	9.20	1.34	0.21	0.35
04288+1802	L1551 NE	51092.9	11.22	2.06	10.97	1.98	10.79	1.97	0.08	0.06
04295+2251	L1536 IRS	51092.9	9.90	1.71	9.77	1.69	9.68	1.74	0.15	0.05
04302+2247	...	51093.0	11.42	1.12	11.13	1.11	10.99	1.10	0.17	0.08
04325+2402	L1535 IRS	51092.9	11.41	1.99	10.94	1.82	10.54	1.60	0.16	0.10
04361+2547	TMR1	51092.9	10.48	2.25	10.29	2.17	10.14	2.10	0.20	0.05
04365+2535	TMC1A	51093.0	10.76	2.87	10.51	2.74	10.33	2.28	0.21	0.15
04381+2540	TMC1	51092.9	11.58	2.27	11.38	2.03	11.26	1.74	0.22	0.07
04489+3042	...	51094.9	10.37	1.56	10.28	1.52	10.25	1.46	0.15	0.13

Table 2. Morphological data for Taurus-Auriga Class I Sources^a

Source Name	f_J (arcsec)	e_J	f_H (arcsec)	e_H	f_K (arcsec)	e_K	Comment ^b
04016+2610	5.23	1.15	11.76	1.19	6.04	1.27	transition
04108+2803A	1.44	1.09	1.89	1.05	2.00	1.06	reddened TTS
04108+2803B	1.86	1.17	1.84	1.06	1.99	1.07	transition?
04158+2805	1.93	1.21	1.90	1.10	2.10	1.10	reddened TTS
04166+2706	6.42	1.55	protostar
04169+2702	14.40	2.43	13.35	1.98	protostar
04181+2655	2.05	1.07	2.18	1.05	transition?
04181+2654B	1.96	1.08	2.25	1.09	protostar
04181+2654A	2.13	1.08	2.10	1.06	protostar
04239+2436	4.94	1.36	2.27	1.06	3.19	1.19	protostar
04248+2612	15.30	2.80	11.20	2.45	11.68	2.43	protostar
04260+2642	1.25	1.09	1.13	1.07	transition?
04264+2433	1.52	1.07	1.77	1.05	1.95	1.04	transition?
04287+1801	2.45	1.16	16.59	1.89	12.39	1.76	protostar
04288+1802	4.17	1.48	2.77	1.18	3.63	1.34	protostar
04295+2251	1.87	1.11	2.14	1.08	2.02	1.05	edge-on disk?
04302+2247	4.26	1.48	3.35	1.27	3.63	1.29	transition
04325+2402	3.62	1.76	9.75	1.69	protostar
04361+2547	2.01	1.25	2.18	1.35	2.77	1.50	protostar
04365+2535	1.57	1.09	2.28	1.18	2.44	1.32	protostar
04368+2537	>25.00	>2.00	protostar
04381+2540	2.07	1.08	2.05	1.06	protostar
04489+3042	1.70	1.07	1.54	1.05	transition?

^aThe columns list the FWHM f and elongation e of gaussian fits to the intensity profile of each source at each wavelength. Based on multiple measurements of each source, the typical error in f is $\pm 0''.2$; the typical error in e is ± 0.1 .

^bThe ‘Comment’ column lists our best estimate of the evolutionary class of each object, true protostars (protostar), objects in transition between class I and class II (transition), edge-on disks, or reddened T Tauri stars.

Table 3. Comparison of infrared and millimeter results

extended in both	extended in neither	extended in mm but not in near-IR continuum	extended in near-IR but not in mm continuum
...	04016+2610
...	04108+2803A
...	04108+2803B
...	04158+2805
04166+2706
04169+2702
...	04181+2655
...	...	04181+2654B	...
...	...	04181+2654A	...
04239+2436
04248+2612
...	04260+2642
...	04264+2433
04287+1801
04288+1802
...	04295+2251
...	04302+2247
04325+2402
04361+2547
...	...	04365+2535	...
04368+2557
...	...	04381+2540	...
...	04489+3042

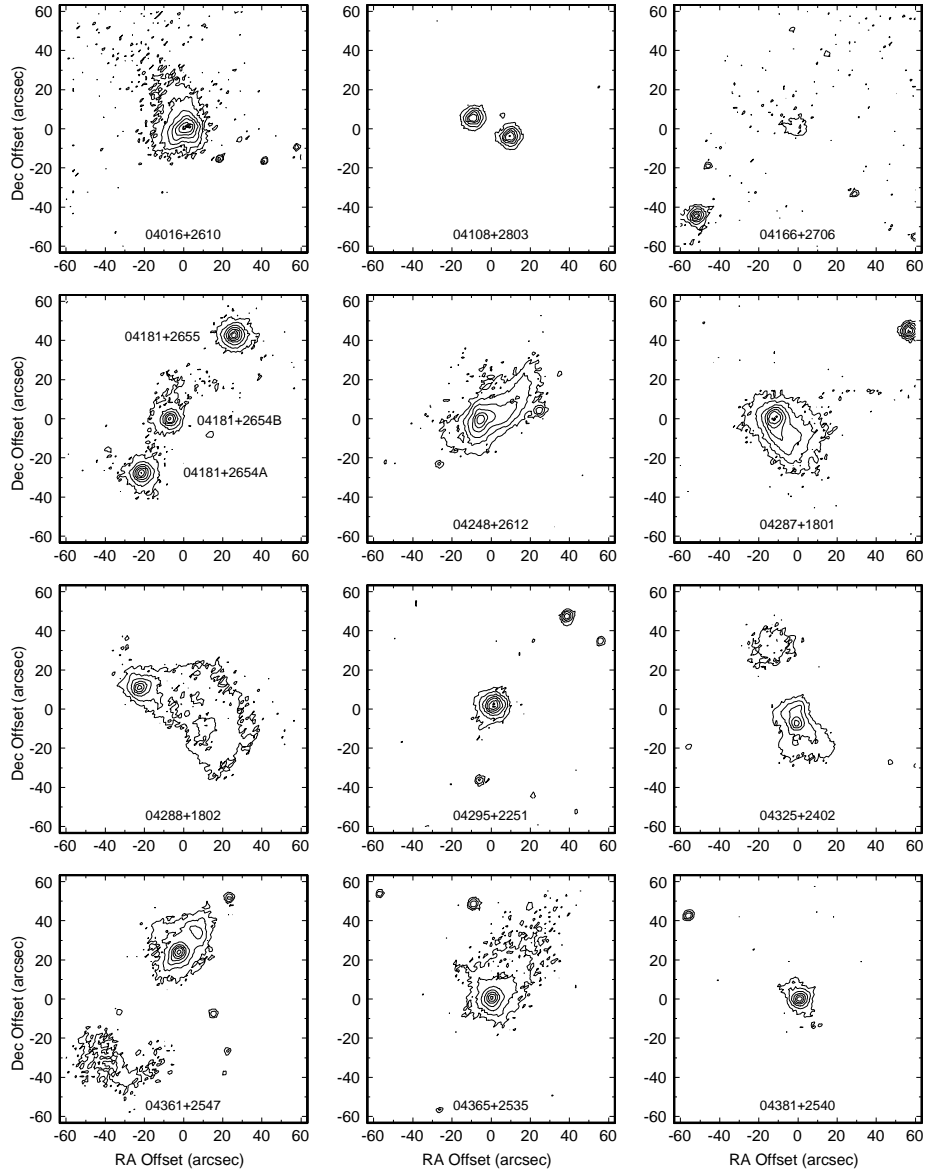


Fig. 1.— K-band contour maps for Taurus-Auriga class I sources. In each panel, north is up and east is to the left. The lowest contour is $\sim 3\sigma$ above the background noise level; the contour spacing is 1 mag.

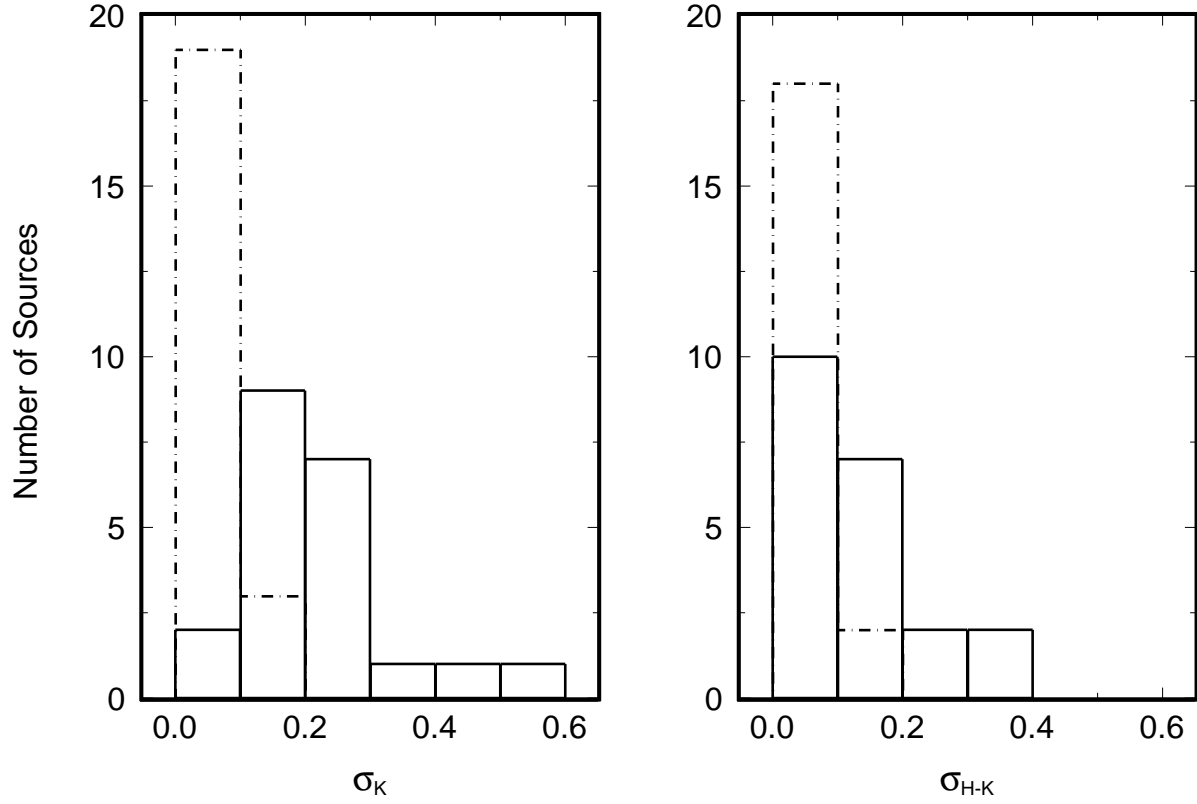


Fig. 2.— Variability of K and H–K in pre-main sequence stars. The left panel shows the distribution of standard deviations σ_K about the mean K magnitude for candidate protostars with 2 or more K measurements (solid line) and for comparison stars in the same field (dot-dashed line). The right panel shows the distribution σ_{H-K} for H–K of candidate protostars (solid line) and of comparison stars (dot-dashed line).

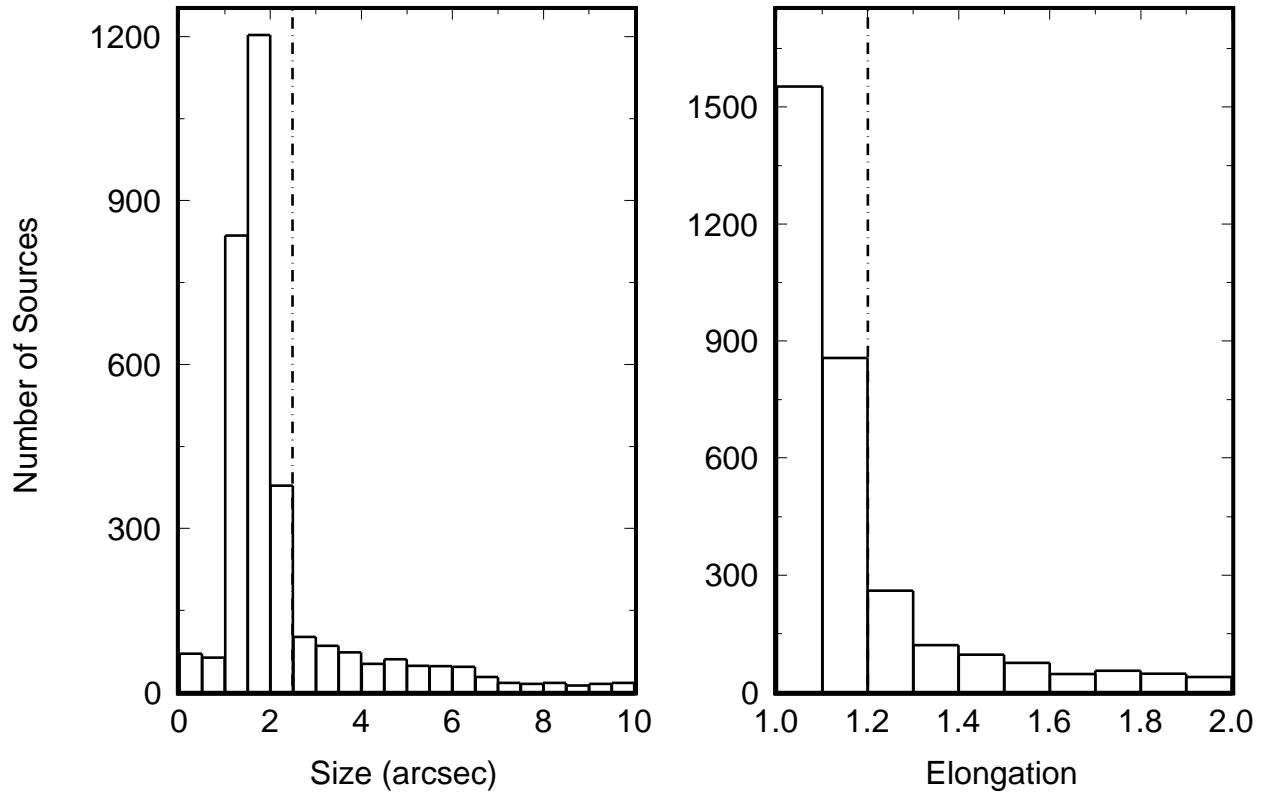


Fig. 3.— Size and elongation histograms for the fields of Taurus-Auriga class I sources. Left panel: size histogram for 3176 sources detected on K-band images of Taurus-Auriga protostars. Right panel: elongation histogram. The dot-dashed line in each panel indicates the division between point sources and extended sources.

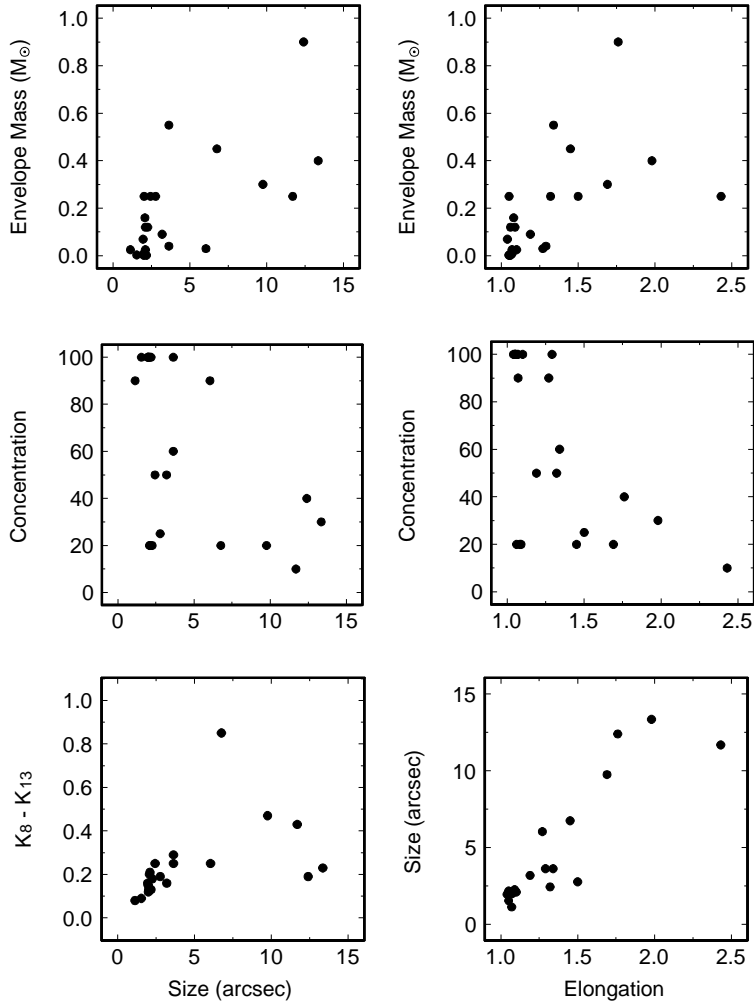


Fig. 4.— Correlations between K-band (size and elongation) and mm continuum properties (envelope mass and concentration) of Taurus-Auriga class I sources. Source elongation correlates well with source size (lower right panel) and mm continuum concentration (middle right panel). The source size correlates well with mm continuum concentration (left middle panel).